Minimally invasive neuroradiologic model of preclinical transient middle cerebral artery occlusion in canines

Cameron Rink*†, Greg Christoforidis†‡, Amir Abduljalil‡, Marinos Kontzialis‡, Valerie Bergdall§, Sashwati Roy*, Savita Khanna*, Andrew Slivka¶, Michael Knopp‡, and Chandan K. Sen*‖

Departments of *Surgery, ‡Radiology, §Veterinary Preventive Medicine, and ¶Neurology, Davis Heart and Lung Research Institute, Ohio State University Medical Center, Columbus, OH 43210

Communicated by Avner Friedman, Ohio State University, July 9, 2008 (received for review April 2, 2008)

Stroke is currently the third leading cause of death in the United States, with approximately 780,000 Americans affected by a new or recurring stroke each year. Although a variety of therapeutic approaches have shown promise in small-animal models of stroke, the vast majority of clinical trials to test the efficacy of such modalities have failed. To bridge the translational gap between laboratory and clinical research, we developed a preclinical model of acute ischemic stroke in dogs. Using a minimally invasive endovascular approach, a platinum coil was intravascularly guided through the vertebrobasilar system under C-arm fluoroscopy to occlude the M1 segment of the middle cerebral artery (MCA) for 1 h. The approach included femoral artery catheterization to access the MCA and therefore eliminated the occurrence of head trauma associated with other preclinical stroke models relying on transorbital or craniectomy approaches. After 1 h of focal MCA ischemia, the coil was retrieved to cause reperfusion, which was verified by arteriograms. At 24 h, T2-weighted coronal magnetic resonance (MR) images were acquired and processed for three-dimensional reconstruction of the brain and its vasculature. Infarction, limited to the area at risk, was noted. Two independent observers calculated the mean percentage hemispherical lesion volumes as follows: observer 1, 30.9 ± 2.1%; observer 2, 31.2 ± 4.3%. Infarct-affected changes in histology were determined by hematoxylin and eosin as well as by Fluoro-Jade staining. This work reports the successful development of a powerful preclinical model of stroke that lends itself to the study of biologic mechanisms as well as to testing experimental therapeutics.

imaging | therapeutics | vascular | stroke | ischemia

Stroke is currently the leading cause of serious long-term disability and the third leading cause of death in the United States, with 780,000 Americans afflicted by a new or recurring stroke each year (1). Although a variety of potential therapeutic agents have shown promise in cell culture and small-animal models of stroke, the vast majority of clinical trials to test the efficacy of such modalities have failed (2, 3). As of 2000, 75 different therapeutic strategies have been tested in acute stroke clinical trials, whereas only 2 of these (tissue plasminogen activator on the basis of the National Institute of Neurological Disorders and Stroke trials and aspirin on the basis of the combined results of the International Stroke Trial and Chinese Acute Stroke Trial) have been widely accepted as of proven benefit (4). Further emblematic of the difficulty in accurately modeling acute ischemic stroke is the 2008 request for applications from the National Institutes of Health and Canadian Stroke Network for Stroke Preclinical Trials Consortia in recognition of "the translational barriers that exist today in stroke research" (5).

To address the gap between laboratory and clinical research, we sought to develop a preclinical model of acute focal ischemia in dogs by using an interventional radiology approach. The advantages of using a canine model are numerous. First, the size and anatomical feature set of the canine brain more closely mimics human brain as compared with those in small-animal stroke models. Dogs have a highly evolved gyrencephalic neocortex with a ratio of white to gray matter that more closely approximates that in humans (6, 7). Second, the neurovascular architecture in dogs accommodates an array of endovascular devices and interventional radiology techniques, permitting a minimally invasive approach to the surgery while providing real-time visualization of occlusion. For example, endovascular middle cerebral artery (MCA) occlusion is made possible by deploying a soft platinum matrix coil clinically used to treat intracranial aneurysms (8). This approach necessitates only two small femoral artery punctures to navigate the neurovasculature and deploy the device in the M1 segment of the MCA under guided fluoroscopy. Finally, the proposed method of MCA occlusion in dogs offers a highly reproducible and relatively inexpensive alternative to nonhuman primate models of acute focal ischemia. Although nonhuman primates are anatomically closer to humans than are dogs, their use poses additional ethical, veterinary, and housing considerations that obligate larger fiscal and personnel requirements (9, 10).

Results

Intuitively, endovascular access to the MCA is via the internal carotid artery (ICA), which contributes to the deficiency of published MCA occlusion models that purposefully explore alternative routes (11). We observed that the ICA to MCA approach was not feasible in dogs because of the tortuosity of the canine ICA [supporting information (SI) Movies S1 and S2]. Our experiments identified that the basilar artery (BA)-to-MCA approach was effective to provide the endovascular access needed for our purposes. Originally, navigation of the canine ICA was attempted with an array of small-diameter microwire (0.010–0.014 inch) and microcatheter systems. However, none were capable of advancing beyond the cavernous portion of the ICA when standard microcatheter techniques were used. Further exploration of the canine cerebrovascular architecture (Fig. 1) revealed the BA approach to be adequately large and straight to accommodate the FASdasher 14 microwire and SL-10 microcatheter. Femoral artery (FA) catheterization allowed access

Author contributions: C.R., G.C., V.B., S.R., and C.K.S. designed research; C.R., G.C., A.A., M. Kontzialis, V.B., S.R., S.K., A.S., and C.K.S. performed research; C.R., G.C., and M. Knopp contributed new reagents/analytic tools; C.R., G.C., A.A., M. Kontzialis, S.R., S.K., A.S., and C.K.S. analyzed data; and C.R., G.C., A.A., V.B., S.R., S.K., A.S., M. Knopp, and C.K.S. wrote the paper.

The authors declare no conflict of interest.

†C.R. and G.C. contributed equally to this work.

‖To whom correspondence should be addressed at: 512 DHLRI, 473 West 12th Avenue, Ohio State University Medical Center, Columbus, OH 43210. E-mail: chandan.sen@osumc.edu.

This article contains supporting information online at www.pnas.org/cgi/content/full/0806678105/DCSupplemental.

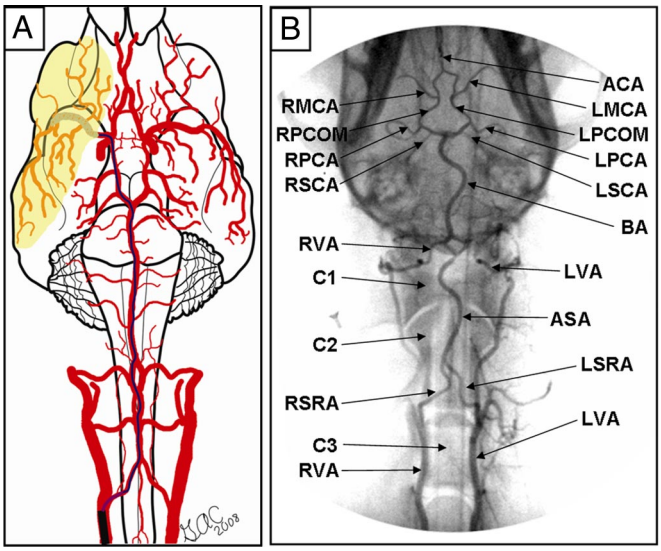

Fig. 1. Canine vertebrobasilar system. The majority of intraluminal MCA occlusion models in animals approach the MCA via the internal carotid. In dogs, this approach is not feasible with microcatheter techniques because of the tortuosity of the internal carotid artery (ICA), which prevents navigation with microwires as small as 0.010 inch in diameter. The alternative approach was to advance a microwire into the basilar artery (BA), along the posterior communicating artery (PCOM), and into the MCA. Subsequently a microcatheter was positioned into the MCA and a 3 × 20 Ultrasoft Matrix2 coil (Boston Scientific) was deployed for 1 h to induce MCA occlusion. After 1 h of occlusion, the coil was retrieved and the MCA territory reperfused as confirmed under fluoroscopy. RVA, right vertebral artery; LVA, left vertebral artery; C3, vertebra C3; LSRA, left spinal ramus artery; RSRA, right spinal ramus artery; C2, vertebra C2; ASA, anterior spinal artery; C1, vertebra C1; BA, basilar artery; LSCA, left superior cerebellar artery; RSCA, right superior cerebellar artery; LPCA, left posterior cerebral artery; RPCA, right posterior cerebral artery; LPCOM, left posterior communicating artery; RPCOM, right posterior communicating artery; LMCA, left middle cerebral artery; RMCA, right middle cerebral artery; ACA, anterior cerebral artery. See Movie S2 for a three-dimensional presentation of the canine vertebrobasilar system.

to the vertebral arteries (VA) that branch off of the left and right subclavian arteries near the aortic arch. The microwire was advanced from either VA into the anterior spinal artery (ASA) via the spinal ramus artery (SRA). The ASA continues intracranially to become the BA. Next, the microwire was directed from the BA around the circle of Willis into either the left or the right MCA depending on which side appeared more favorable to access under C-arm fluoroscopy. The potential of posterior communicating (PCOM) artery and BA vasospasm necessitated constant monitoring of contrast filling under fluoroscopy to assure that neither was unintentionally occluded by the microwire or microcatheter. Inadvertent BA and PCOM occlusion was documented in preliminary studies. To reduce the risk of inadvertent occlusion, the matrix coil was quickly deployed into the MCA upon successful tracking of the microcatheter across the PCOM (Fig. 2*A*). After placement of the matrix coil in the M1 segment of the MCA, the microcatheter was then retreated to the origin of the BA. Successful MCA occlusion was verified by ICA injection of contrast agent under fluoroscopy. During 1-h MCA occlusion, both ICAs were routinely subjected to arteriograms to confirm occlusion of the ipsilateral MCA and opacification of the contralateral hemisphere (Fig. 2*B*). After 1 h of occlusion, the matrix coil was retrieved and patency of the MCA territory confirmed reperfusion (Fig. 2*C*). Slower than normal filling of the reperfused MCA was documented and presumed to be a consequence of vasospasm. A postreperfusion BA arteriogram was performed to confirm opacification of the PCOMs and both MCAs. Physiologic parameters, including heart rate, respiration rate, oxygen saturation, and end-tidal CO_2 were monitored and maintained stable before, during, and after MCA occlusion (Table S1).

At 24 h after MCA reperfusion, high-resolution T2-weighted images of coronal brain slices from 3-T MRI revealed infarct associated with the region of the cerebral cortex supplied by the MCA (Figs. 3 and 4). To quantitate infarct volume, manual planimetry was performed to delineate the infarct region and the ipsilateral and contralateral hemispheres. Hemispheric volumes were determined from T2-weighted images by use of the following neuroanatomic landmarks: falx cerebri, pineal gland, fissura longitudinalis, infundibulum, sylvian aqueduct, and third ventricle. Lesion areas were then summed and multiplied by the slice gap thickness to obtain an infarct volume uncorrected for edema. A substantial midline shift, evidenced by the displacement of the third ventricle, is characteristic of the supratentorial lesion. As a result, the relative hemispherical size is distorted which in turn leads to a misrepresentation of true hemispherical infarct volume. Because of the strong presence of edema induced swelling in canine brain at 24 h after MCA reperfusion, we used a previously reported method for edema corrected lesion volume calculation (12). This calculation is based on the following three assumptions: (*i*) compression of the contralateral hemisphere is comparable to compression of the entire healthy brain tissue, whereas the lesion is not compressed; (*ii*) the contralateral hemisphere is compressed to the same extent as the affected

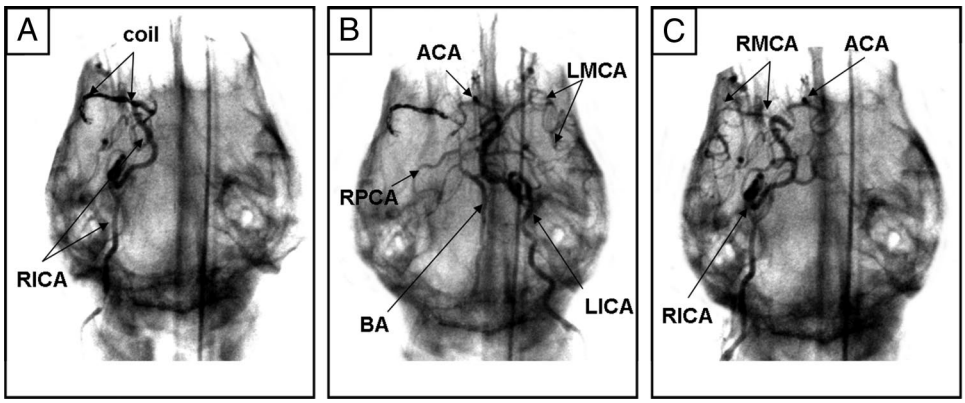

Fig. 2. C-arm fluoroscopy enabled real-time verification of MCA occlusion and reperfusion in the canine brain. (*A*) The matrix coil was deployed into the RMCA, occluding the M1 segment, as confirmed by RICA contrast injection. (*B*) LICA angiography demonstrated that the LMCA was still intact, along with the ACA, BA, and RPCA. The RMCA still did not fill. (*C*) After 1-h occlusion, the matrix coil was retrieved and RICA arteriogram confirmed that the RMCA had reperfused.

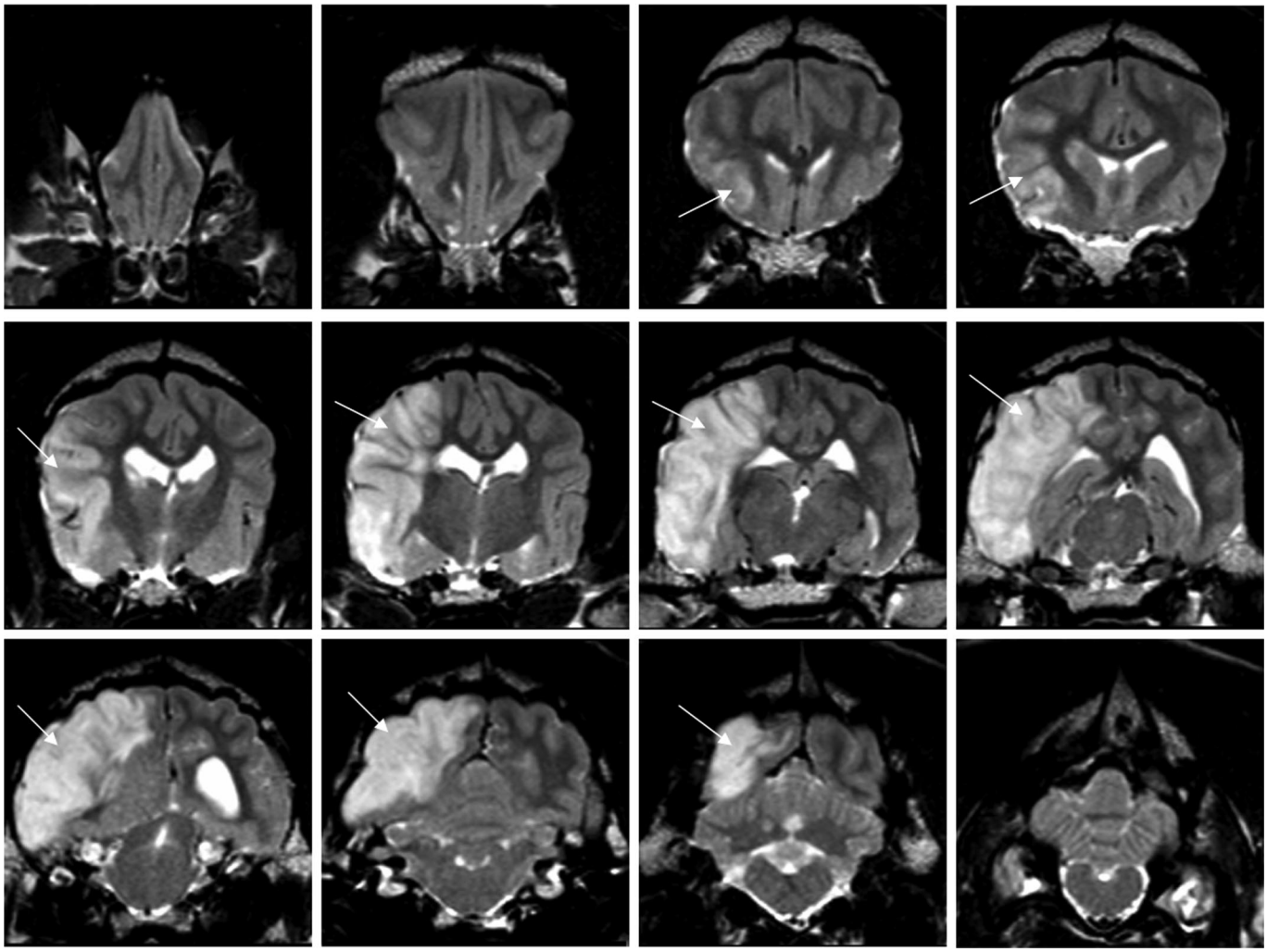

Fig. 3. Coronal slices of MCA territory stroke-induced brain lesion. T2-weighted MRI (TR = 3000 ms, TE = 100 ms, field of view = 145 mm, slice thickness = 3.0 mm, echo train length = 15, acquisition matrix = 256 × 256, number of averages = 2) was performed 24 h after reperfusion of the MCA using a Phillips 3-T system. Coronal slices demonstrating cortical edema (arrow) are ordered from anterior (*Top Left*) to posterior (*Bottom Right*) cortex.

hemisphere is extended (total brain volume does not change); and (*iii*) volume extension occurs only within the lesion, not in the unaffected tissue. Taking these factors into account, the mean percentage hemispherical infarct volume corrected for edema in the four dogs as reviewed by two independent observers was 30.9 ± 2.1% and 31.2 ± 4.3%, respectively (Fig. 5). Three-dimensional reconstruction of axial MRI slices using Osirix software (open source, The Osirix Foundation) provided a clear visual representation of infarct size in relation to hemispherical volume (Movie S3). Hematoxylin and eosin staining of the stroke-induced infarct tissue of the neocortex at the 24-h time point revealed condensed pyknotic nuclei as compared with contralateral control tissue (Fig. 6 *A*, *B*, *D*, and *E*). Positive Fluoro-Jade immunofluorescence staining indicated neuronal degeneration in infarct affected tissue as compared with contralateral controls (Fig. 6 *C* and *F*).

Discussion

The intraluminal suture model of MCA occlusion in rats was reported by Koizumi *et al.* in 1986 and later modified by Longa *et al.* in 1989, and introduced a noninvasive small-animal model of acute focal ischemia (13, 14). To this day, the model continues to be the most frequently used method to test potential therapeutic stroke agents *in vivo* (15). Several variations of techniques and approaches to induce MCA occlusion in rodents have been published since the model's inception; however, none have been as widely accepted (16–18). Despite the popularity of the intraluminal suture model, there remain significant limitations to the approach that have been extensively documented in the literature and contribute to the high degree of variability in lesion volume and location across and within studies (2, 15, 19–23). First, real-time placement of the occluder in the rodent MCA cannot be visualized. Consequently, overshooting or undershooting the MCA origin is expected to be a common occurrence that may contribute to variability in lesion volume outcomes. Laser Doppler flowmetry (LDF) clearly improves the reliability of occluder placement; however, LDF provides information on the relative decrease in blood flow at only a single point, thereby making it difficult to determine whether the territory is fully or only partially occluded. A significant advantage of the canine guided fluoroscopy approach is the appreciation of M1 segment MCA occlusion in real time using angiograms. This procedure allows visualization of the entire ischemic territory and confirms partial or full occlusion of the MCA. Further contributing to the variability of stroke lesion volume in the intraluminal thread model is the potential for premature reperfusion of the MCA territory, which has been documented to occur in approximately 25% of experimental animals (15).

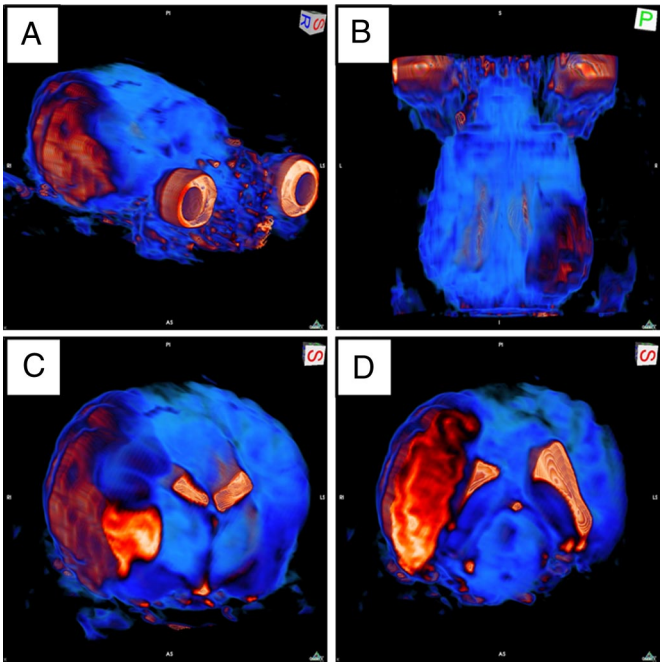

Fig. 4. Volumetric reconstruction of stroke-induced infarct lesion. T2-weighted MRI coronal slices (acquisition details in Fig. 3 legend) were volume rendered. Color contrast from blue to orange to white represents increasing signal intensity. The eyes have been kept in the field of view for orientation purposes (A and B). Stroke-induced infarct appears orange throughout a large portion of the right hemisphere. (*A*) Oblique view. (*B*) Anterior/posterior view. Coronal sectioning through the brain reveals MCA territory infarct and ventricular compression in the right hemisphere. (*C* and *D*) Oblique view of right hemishphere. See Movie S3 for a three-dimensional presentation of this figure.

Although premature reperfusion was not encountered in this study, repeated monitoring of the MCA territory via C-arm fluoroscopy allowed for adjustment of the matrix coil as needed to ensure complete occlusion of the MCA throughout the ischemic event. Finally, it has been reported in the intraluminal thread model that after placement of the filament tip in the proximal MCA, the remaining filament in the ICA is occlusive to the anterior choroid artery and the hypothalamic artery, thereby producing unintentional subcortical lesions (24). In the currently reported preclinical model, we have documented that occlusion is specific to the MCA-supplied territory and that by retreating the microcatheter to the BA origin we can prevent

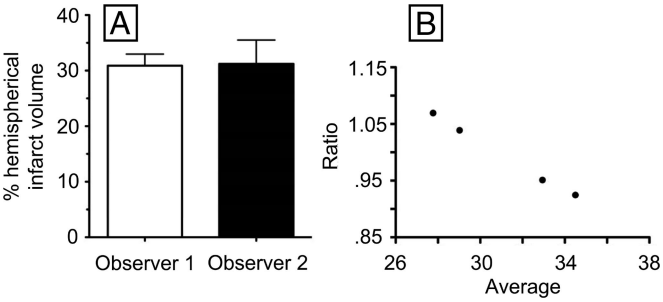

Fig. 5. Stroke-induced infarct volume as determined by MRI. After 24-h reperfusion, coronal images were analyzed to determine the volume of the stroke-induced lesion. Two observers calculated infarct volume independently. (*A*) Mean percentage hemispherical lesion volumes ($n = 4$): observer 1, 30.9 ± 2.1; observer 2, 31.2 ± 4.3. (*B*) Bland–Altman observer comparison of ratio (observer 1/observer 2) versus average, bias = 1.0003 ± 0.066.

unintentional occlusion of arteries, such as the PCOM, which remain patent under fluoroscopy.

The high degree of variability in lesion volume associated with the intraluminal suture model is not limited to experimentation in small animals such as rodents. In translating the intraluminal suture model to nonhuman primates, Freret *et al.* reported a 58% standard deviation around the mean infarct volume from marmosets ($n = 4$) subjected to transient MCA occlusion (25). In contrast, the standard deviation around the mean ($n = 4$) in dogs when the current matrix coil approach is used was found to be less than 15% for both observers. Similarly, other endovascular models using the ICA route to MCA occlusion in nonhuman primates have reported large standard deviations in infarct volume across animals (26, 27). The appreciably tighter standard deviation in stroke-induced lesion volumes when our model is used suggests that fewer experimental animals would be required to achieve statistical significance in studying potential therapeutic candidates. As it relates to other large-animal models of MCA occlusion, our proposed method of endovascular occlusion differs in that it offers a minimally invasive approach. Several variations of transorbital MCA occlusion via vessel clamp in nonhuman primates have been reported (28–32). Although variants of such models have reported highly reproducible infarct volumes, these models necessitate an invasive approach including removal of the orbital globe, transection of the optic nerve and opthalmic artery, and craniectomy of the posteromedial orbit (30). Thus far, the effects of the orbital wound and trauma-induced inflammatory response have not been resolved separately from the stroke-induced pathologic conditions. The craniectomy approach to model stroke in a preclinical setting is also associated with severe head trauma, changes in intracranial pressure, and cerebrospinal fluid loss (33, 34). Because stroke in humans is not necessarily associated with head trauma, the traumatic aspect of invasive surgery may be viewed as a major confounding factor. The close proximity of the trauma to the stroke site in these invasive models, including removal of the skull and dura covering the anterior circle of Willis, poses significant limitations. The minimally invasive nature of the surgical approach described in the current study therefore represents a major strength. Of further consideration when working with nonhuman primates is the increased cost resulting from stringent enrichment program and housing guidelines (35, 36). Although the standard of care remains the same, the relative cost of canine environmental enrichment and housing is considerably less compared with that for nonhuman primates.

Advantages aside, the endovascular model as described is not without its own unique set of challenges and potential pitfalls. First, there was a steep learning curve to navigating the canine intracranial vasculature. Several animals were required early in the model development to familiarize the surgeon with the tactile skill set and tools necessary to achieve successful endovascular navigation. Second, the canine vertebrobasilar system is prone to microcatheter and microwire arresting vasospasm. Significant precaution must be taken to avoid prolonged exposure of the microcatheter to the PCOM and distal BA. Microwire movement must also be limited to the purposeful advancement of the wire to the MCA origin as quickly as possible to avoid spasm. In the case of spasm occurring, waiting for it to resolve for a short interval (5–10 min) or delivering a small dose of spasmolytic agent generally overcame the problem. Finally, in some dogs, MCA cannulation was simply not possible because of variations in their cerebrovascular anatomy. In this instance, and when appropriate, catheters and wires were removed, and the dogs were allowed to recover and were transferred out of the study.

Successful translation of stroke therapeutics research from the laboratory to the clinic has failed to meet expectations. Con-

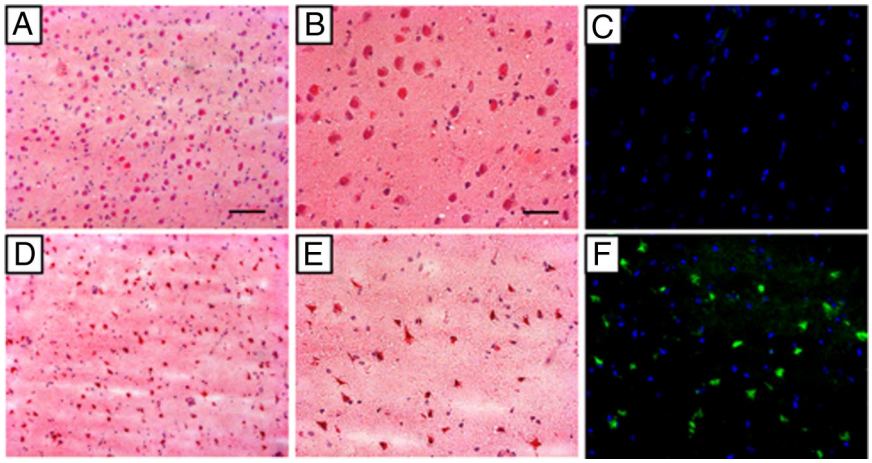

Fig. 6. Histologic analysis of poststroke infarct and control tissue. Twenty-four hours after MRI, dogs ($n = 4$) were euthanized and brain tissue was cryosectioned for histologic analyses. (*A* and *D*) Hematoxylin and eosin (H&E) staining of noninfarcted contralateral hemisphere tissue (*A*) and infarcted stroke tissue (*D*) at ×10 magnification. (*B* and *E*) Staining of noninfarcted contralateral hemisphere tissue (*B*) and infarcted stroke tissue (*E*) at ×20 magnification. (*C* and *F*) Nucleus (blue, DAPI) and degenerative neuron staining (green, Fluoro Jade) of noninfarcted contralateral hemisphere tissue (*C*) and infarcted stroke tissue (*F*) at ×20 magnification. (Scale bars: *A* and *D*, 0.1 mm; *B*, *C*, *E*, and *F*, 0.05 mm.)

tributing to the discrepancy in laboratory and clinical results are the limitations of small-animal models to produce tightly reproducible surgical procedures across and within studies, and the vast anatomical and functional differences between small and large mammalian brains. To date, several large-animal models of stroke in nonhuman primates have used an invasive transorbital approach which introduces trauma associated complications in addition to the cost-prohibitive nature and ethical considerations associated with the use of nonhuman primate subjects. The endovascular canine model of transient MCA occlusion reported herein serves as a powerful preclinical stroke model benefiting from guided fluoroscopic occlusion of the MCA, and high interanimal reproducibility in a cost-effective large-animal setting.

Materials and Methods

Endovascular Canine MCA Occlusion. All experimentation was approved by the Institutional Laboratory Animal Care and Use Committee of Ohio State University. One day before percutaneous intervention, mongrel dogs ($n = 4$) with a body weight of 20–30 kg received a 300-mg loading dose of clopidogrel. On the day of surgery, the animals were sedated with telazol (6 mg/kg body weight administered intramuscularly, volume <3 ml) and anesthetized (1.5–2.0% isoflurane). Continuous cardiac rhythm, respiration rate, end-tidal CO_2, and oxygen saturation were monitored for control of physiologic parameters. Canine body temperature was maintained around the normal range of 38–39.2°C by using a convective warming system (Gaymar Thermacare).

Bilateral common femoral artery access was obtained by using 5 French sheaths (ArrowGE Healthsystems) a 5-Fr guide catheter (Boston Scientific) was advanced into the vertebral artery (VA) and was hooked up to a pressurized drip. The animal was administered 2,000 units of heparin as a bolus. A 4 French catheter (Boston Scientific) was then placed in the right vertebral artery to provide access into the basilar artery system and allow for periodic infusion of spasmolytic agents as needed (papaverine 0.3 mg/ml delivered in 1-ml aliquots). Arteriography allowed for documentation of vasodilatation in the intended territory. Microcatheter techniques were then used to access the MCA via the circle of Willis (Fig. 1). Through the vertebral artery (VA) guide catheter an SL-10 microcatheter (Boston Scientific) with a microwire was advanced into the MCA. Once the microcatheter was in place, an embolic coil (3 × 20 Ultrasoft Matrix2 Platinum Coil, Boston Scientific) was delivered into either MCA to include the entire M1 segment. The 4F catheter and the 5F catheter were then used to perform digital subtraction angiograms (DSAs) of the internal carotid arteries and the vertebrobasilar circulation to confirm complete occlusion of the MCA by fluoroscopic contrast injection without evidence for either circle of Willis collaterals or any pial collateral formation that may have developed during the occlusion. The coil was repositioned if necessary to achieve complete occlusion. Angiographic evidence for incomplete occlusion or pial collateral formation reconstituting the occluded territory was considered exclusion criterion for MRI analysis. Once the coil was positioned, the microcatheter was drawn back into the third spinal arterial ramus. ICA and VA DSAs were repeated every 15 min to confirm continued occlusion. Occlusion of the MCA lasted for 1 h. At the end of the transient occlusion, the microcatheter was advanced back into the MCA and the coil was captured and retrieved. The VA and ICA DSAs were repeated to confirm reperfusion of the occluded territory. The catheters were then removed. A blood draw for activated clotting time was then obtained. Depending on the result of the activation time, a weight-based calculated dose of protamine was delivered to the dog to reverse the effects of heparinization. The sheaths were then removed and pressure was applied at the arteriotomy sites for hemostasis. The dog was then brought out of anesthesia and extubated, and the arteriotomy sites were periodically checked for hematoma. Postoperative veterinary care was provided to the dogs for 24 h before MRI.

MRI. Evaluation of the infarct lesion was accomplished by using 3-T MRI (Philips Healthcare) 24 h after MCA reperfusion. The animal was sedated with telazol (6 mg/kg of body weight, administered intramuscularly, volume <3 ml) and anesthetized (1.5–2.0% isoflurane) throughout the MRI scans (≈1 h). While dogs were under anesthesia in the magnet, the heart rate, respiratory rate, and body temperature were monitored. All MRI was performed under the guidance and supervision of a trained technician at our Wright Center of Innovation for Biomedical Imaging (Columbus, OH). The image processing software ImageJ (National Institutes of Health, Bethesda, MD) was used for infarct volume calculation from coronal T2-weighted MR images (3-mm slice thickness). Raw MR images were converted to standard Digital Imaging and Communications in Medicine (DICOM) format and transferred to an image-processing workstation. After appropriate software contrast enhancement of the images, manual planimetry was performed by two independent observers to delineate the infarct region, ipsilateral hemisphere, and contralateral hemisphere. We used this technique to quantitate stroke injury as a fraction of contralateral hemisphere and total brain volume. Correction for edema-induced midline shift in hemispherical volume was incorporated into infarct volume calculations as described previously (12). Interobserver reproducibility was assessed by using the Bland–Altman statistic (37).

Histology. Dogs were euthanized (Euthasol Euthanasia Solution, IV, 1 ml/4.6 kg; Virbac AH Inc.) immediately after MRI. Next, necropsy was performed to isolate the brain. Continuous 3-mm coronal slices were collected throughout the ipsilateral and contralateral hemispheres using a canine brain matrix. Sections were rinsed in PBS, embedded in OCT compound (Sakura Finetek), and frozen at −80°C. OCT-embedded slices were subsequently cut in 10-μm-thick sections on a Leica CM 3050 S cryostat (Leica Microsystems) and mounted onto slides for histologic determinations. Hematoxylin and eosin staining of frozen canine brain tissue was performed to contrast gross stroke pathology in infarct-affected and contralateral control tissue.

Fluoro-Jade is an anionic fluorochrome capable of selectively staining degenerating neurons in brain slices. Compared with conventional methodologies, Fluoro-Jade is a sensitive and more definitive marker of neuronal degeneration than Nissl type stains, while also being comparably sensitive yet considerably simpler and more reliable than suppressed silver techniques (38). To determine neuronal degeneration, frozen brain sections (10 μm) were stained by using the Fluoro-Jade procedure (39). Tissue sections were analyzed by fluorescence microscopy (Axiovert 200M) and images were captured using Axiovert v4.6 software (Zeiss).

ACKNOWLEDGMENTS. This work was supported by National Institutes of Health Grant NS42617 (to C.K.S.) and American Heart Association Grant 0615240B (to C.R.).

1. Rosamond W, *et al.* (2008) Heart disease and stroke statistics—2008 update: A report from the American Heart Association Statistics Committee and Stroke Statistics Subcommittee. *Circulation* 117:e25–e146.
2. Lodder J (2000) Neuroprotection in stroke: Analysis of failure, and alternative strategies. *Neurosci Res Commun* 26:173–179.
3. Van Reempts JBM (2000) Animal models of stroke: Compromise between consistency and clinical relevance? *Neurosci Res Commun* 26:161–172.
4. Kidwell CS, Liebeskind DS, Starkman S, Saver JL (2001) Trends in acute ischemic stroke trials through the 20th century. *Stroke* 32:1349–1359.
5. National Institutes of Health and Canadian Stroke Network (2007) *Stroke Preclinical Trials Consortia (U01)* (National Institutes of Health, Bethesda, MD), RFA-NS-08-001, pp. 1–18.
6. Zhang K, Sejnowski TJ (2000) A universal scaling law between gray matter and white matter of cerebral cortex. *Proc Natl Acad Sci USA* 97:5621–5626.
7. Traystman RJ (2003) Animal models of focal and global cerebral ischemia. *ILAR J* 44:85–95.
8. Raymond J, Darsaut T, Salazkin I, Gevry G, Bouzeghrane F (2008) Mechanisms of occlusion and recanalization in canine carotid bifurcation aneurysms embolized with platinum coils: An alternative concept. *AJNR Am J Neuroradiol* 29:745–752
9. Quigley, M (2007) Non-human primates: The appropriate subjects of biomedical research? *J Med Ethics* 33:655–658.
10. Bhogal N, Hudson M, Balls M, Combes RD (2005) The use of non-human primates in biological and medical research: Evidence submitted by FRAME to the Academy of Medical Sciences/Medical Research Council/Royal Society/Wellcome Trust Working Group. *Altern Lab Anim* 33:519–527.
11. Connors JJ, Wojak JC (1999) *Interventional Neuroradiology: Strategies and Practical Techniques* (Saunders, Philadelphia).
12. Loubinoux I, *et al.* (1997) Spreading of vasogenic edema and cytotoxic edema assessed by quantitative diffusion and T2 magnetic resonance imaging. *Stroke* 28:419–426; discussion 426–427.
13. Koizumi J, Yoshida Y, Nakazawa T, Ooneda G (1986) Experimental studies of ischemic brain edema: I: A new experimental model of cerebral embolism in rats in which recirculation can be introduced in the ischemic area. *Jpn J Stroke* 8:1–8.
14. Longa EZ, Weinstein PR, Carlson S. Cummins R (1989) Reversible middle cerebral artery occlusion without craniectomy in rats. *Stroke* 20:84–91.
15. Schmid-Elsaesser R, Zausinger S, Hungerhuber E, Baethmann A, Reulen HJ (1998) A critical reevaluation of the intraluminal thread model of focal cerebral ischemia: Evidence of inadvertent premature reperfusion and subarachnoid hemorrhage in rats by laser-Doppler flowmetry. *Stroke* 29:2162–2170.
16. Busch E, Kruger K, Hossmann KA (1997) Improved model of thromboembolic stroke and rt-PA induced reperfusion in the rat. *Brain Res* 778:16–24.
17. Gerriets T, *et al.* (2003) The macrosphere model: Evaluation of a new stroke model for permanent middle cerebral artery occlusion in rats. *J Neurosci Methods* 122:201–211.
18. Umemura K, Nakashima M (1993) A new model of middle cerebral artery thrombosis in rats (translated from Japanese). *Yakubutsu Seishin Kodo* 13:9–17.
19. Belayev L, Alonso OF, Busto R, Zhao W, Ginsberg MD (1996) Middle cerebral artery occlusion in the rat by intraluminal suture. Neurological and pathological evaluation of an improved model. *Stroke* 27:1616–622; discussion 1623.
20. Garcia JH, Wagner S, Liu KF, Hu XJ (1995) Neurological deficit and extent of neuronal necrosis attributable to middle cerebral artery occlusion in rats. Statistical validation. *Stroke* 26:627–634; discussion 635.
21. Kawamura S, Li Y, Shirasawa M, Yasui N, Fukasawa H (1994) Reversible middle cerebral artery occlusion in rats using an intraluminal thread technique. *Surg Neurol* 41:368–373.
22. Kawamura S, Yasui N, Shirasawa M, Fukasawa H (1991) Rat middle cerebral artery occlusion using an intraluminal thread technique. *Acta Neurochir (Wien)* 109:126–132.
23. Memezawa H, Smith M L, Siesjo BK (1992) Penumbral tissues salvaged by reperfusion following middle cerebral artery occlusion in rats. *Stroke* 23:552–559.
24. Gerriets T, *et al.* (2004) Complications and pitfalls in rat stroke models for middle cerebral artery occlusion: A comparison between the suture and the macrosphere model using magnetic resonance angiography. *Stroke* 35:2372–2377.
25. Freret T, *et al.* (2007) Intraluminal thread model of focal stroke in the non-human primate. *J Cereb Blood Flow Metab* 28:786–796.
26. Gao H, Liu Y, Lu S, Xiang B, Wang C (2006) A reversible middle cerebral artery occlusion model using intraluminal balloon technique in monkeys. *J Stroke Cerebrovasc Dis* 15:202–208.
27. Liu Y, *et al.* (2007) Serial diffusion tensor MRI after transient and permanent cerebral ischemia in nonhuman primates. *Stroke* 38:138–145.
28. Crowell RM, Olsson Y, Klatzo I, Ommaya A (1970) Temporary occlusion of the middle cerebral artery in the monkey: Clinical and pathological observations. *Stroke* 1:439–448.
29. Frazee JG, *et al.* (1998) Retrograde transvenous neuroperfusion: A back door treatment for stroke. *Stroke* 29:1912–1916.
30. Huang J, *et al.* (2000) A modified transorbital baboon model of reperfused stroke. *Stroke* 31:3054–3063.
31. Young AR, *et al.* (1997) Early reperfusion in the anesthetized baboon reduces brain damage following middle cerebral artery occlusion: A quantitative analysis of infarction volume. *Stroke* 28:632–637; discussion 637–638.
32. Ducruet AF, *et al.* (2007) Pre-clinical evaluation of an sLe x-glycosylated complement inhibitory protein in a non-human primate model of reperfused stroke. *J Med Primatol* 36:375–80.
33. Goettler CE, Tucci KA (2007) Decreasing the morbidity of decompressive craniectomy: The Tucci flap. *J Trauma* 62:777–778.
34. Jiang JY, *et al.* (2005) Efficacy of standard trauma craniectomy for refractory intracranial hypertension with severe traumatic brain injury: A multicenter, prospective, randomized controlled study. *J Neurotrauma* 22:623–628.
35. Bloomsmith MA, Brent LY, Schapiro SJ (1991) Guidelines for developing and managing an environmental enrichment program for nonhuman primates. *Lab Anim Sci* 41:372–377.
36. Storey PL, Turner PV, Tremblay JL (2000) Environmental enrichment for rhesus macaques: A cost-effective exercise cage. *Contemp Top Lab Anim Sci* 39:14–16.
37. Bland JM, Altman DG (1999) Measuring agreement in method comparison studies. *Stat Methods Med Res* 8:135–160.
38. Schmued LC, Albertson C, Slikker W, Jr (1997) Fluoro-Jade: A novel fluorochrome for the sensitive and reliable histochemical localization of neuronal degeneration. *Brain Res* 751:37–46.
39. Khanna S, *et al.* (2005) Neuroprotective properties of the natural vitamin E alpha-tocotrienol. *Stroke* 36:2258–2264.